

Sub-100 W picosecond output from a phase-conjugate Nd:YVO₄ bounce amplifier

K. Nawata¹, M. Okida¹, K. Furuki¹, K. Miyamoto¹, and T. Omatsu^{1,2,*}

¹Department of Information and Image Sciences, Chiba University, 1-33, Yayoi-cho, Inage-ku, Chiba, 263-8522, Japan

²PREST, Japan Science and Technology Agency, 4-1-8, Honcho, Kawaguchi, Saitama, Japan
[*omatsu@faculty.chiba-u.jp](mailto:omatsu@faculty.chiba-u.jp)

Abstract: We demonstrated >80 W picosecond output at a pulse repetition frequency of 100 MHz from a dual Nd:YVO₄ amplifier laser system consisting of a phase-conjugate Nd:YVO₄ bounce amplifier combined with a second diode-side-pumped Nd:YVO₄ bounce amplifier. The output exhibited high quality spatial form with $M^2 < 1.8$ and a pulse duration (FWHM) of 9.2 ps. A peak power of >7.4 MW with an average power of 78.5 W was also achieved at a pulse repetition frequency of 1.0 MHz.

©2009 Optical Society of America

OCIS codes: (190.5040) Phase conjugation; (320.5390) Picosecond phenomena; (140.3580) Lasers, solid-state; (140.3280) Laser amplifiers.

References and links

1. L. McDonagh, R. Wallenstein, and A. Nebel, "111 W, 110 MHz repetition-rate, passively mode-locked TEM₀₀Nd:YVO₄ master oscillator power amplifier pumped at 888 nm," *Opt. Lett.* **32**(10), 1259–1261 (2007).
2. S. Tokita, J. Kawanaka, Y. Izawa, M. Fujita, and T. Kawashima, "23.7-W picosecond cryogenic-Yb:YAG multipass amplifier," *Opt. Express* **15**(7), 3955–3961 (2007).
3. M. Siebold, M. Hornung, J. Hein, G. Paunescu, R. Sauerbrey, T. Bergmann, and G. Hollemann, "A high-average-power diode-pumped Nd:YVO₄ regenerative laser amplifier for picosecond-pulses," *Appl. Phys. B* **78**, 387–390 (2004).
4. J. Kleinbauer, R. Knappe, and R. Wallenstein, "A powerful diode-pumped laser source for micro-machining with ps pulses in the infrared, the visible and the ultraviolet," *Appl. Phys. B* **80**(3), 315–320 (2005).
5. A. Agnesi, L. Carra, F. Pirzio, G. Reali, A. Tomaselli, D. Scarpa, and C. Vacchi, "Amplification of a low-power picosecond Nd:YVO₄ laser by a diode-laser, side-pumped, grazing-incidence slab amplifier," *IEEE J. Quantum Electron.* **42**(8), 772–776 (2006).
6. G. Smith, P. C. Shardlow, and M. J. Damzen, "High-power near-diffraction-limited solid-state amplified spontaneous emission laser devices," *Opt. Lett.* **32**(13), 1911–1913 (2007).
7. A. Minassian, B. A. Thompson, G. Smith, and M. J. Damzen, "High-power scaling (>100 W) of a diode-pumped TEM₀₀ Nd:GdVO₄ laser system," *IEEE J. Quantum Electron.* **11**(3), 621–625 (2005).
8. N. Shiba, Y. Morimoto, K. Furuki, Y. Tanaka, K. Nawata, M. Okida, and T. Omatsu, "Picosecond master-oscillator, power-amplifier system based on a mixed vanadate phase conjugate bounce amplifier," *Opt. Express* **16**(21), 16382–16389 (2008).
9. Y. Ojima, K. Nawata, and T. Omatsu, "Over 10-watt picosecond diffraction-limited output from a Nd:YVO₄ slab amplifier with a phase conjugate mirror," *Opt. Express* **13**(22), 8993–8998 (2005).
10. K. Nawata, Y. Ojima, M. Okida, T. Ogawa, and T. Omatsu, "Power scaling of a pico-second Nd:YVO₄ master-oscillator power amplifier with a phase-conjugate mirror," *Opt. Express* **14**(22), 10657–10662 (2006).
11. T. Omatsu, K. Nawata, M. Okida, and K. Furuki, "MW ps pulse generation at sub-MHz repetition rates from a phase conjugate Nd:YVO₄ bounce amplifier," *Opt. Express* **15**(15), 9123–9128 (2007).
12. L. Lombard, A. Brignon, J. P. Huignard, E. Lallier, G. Lucas-Leclin, P. Georges, G. Pauliat, and G. Roosen, "Diffraction-limited polarized emission from a multimode ytterbium fiber amplifier after a nonlinear beam converter," *Opt. Lett.* **29**(9), 989–991 (2004).
13. N. V. Bogodaev, L. I. Ivleva, A. S. Korshunov, A. V. Mamaev, N. N. Polozkov, and A. A. Zozulya, "Geometry of a self-pumped passive ring mirror in crystals with strong fanning," *J. Opt. Soc. Am. B* **10**(6), 1054–1059 (1993).
14. N. Huot, J. M. C. Jonathan, G. Roosen, and D. Rytz, "Characterization and optimization of a ring self-pumped phase-conjugate mirror at 1.06 μm with BaTiO₃:Rh," *J. Opt. Soc. Am. B* **15**(7), 1992–1999 (1998).
15. T. Omatsu, K. Nawata, D. Sauder, A. Minassian, and M. J. Damzen, "Over 40-watt diffraction-limited Q-switched output from neodymium-doped YAG ceramic bounce amplifiers," *Opt. Express* **14**(18), 8198–8204 (2006).
16. J. C. Bermudez, V. J. Pinto-Robledo, A. V. Kir'yanov, and M. J. Damzen, "The thermo-lensing effect in a grazing incidence, diode-side-pumped Nd:YVO₄ laser," *Opt. Commun.* **210**(1-2), 75–82 (2002).

17. X. Yan, M. Gong, F. He, Q. Liu, X. Fu, and D. Wang, "Numerical modeling of the thermal lensing effect in a grazing-incidence laser," *Opt. Commun.* **282**(9), 1851–1857 (2009).
18. M. Okida, A. Tonouchi, M. Itoh, T. Yatagai, and T. Omatsu, "Thermal-lens measurement in a side-pumped 1.3 mm Nd:YVO₄ bounce laser," *Opt. Commun.* **277**(1), 125–129 (2007).

1. Introduction

High-power picosecond lasers have been intensively investigated because they have the potential to be used in various applications, including nonlinear frequency-conversion processes, nonlinear microscopy, and microfabrication [1,2]. Most such lasers have been based on a regenerative amplifier scheme and consequently their pulse repetition frequencies have been limited to about 100 kHz [3,4].

Side-pumped bounce amplifiers based on a neodymium-doped vanadate slab such as Nd:YVO₄ [5,6], Nd:GdVO₄ [7], and Nd:Gd_xY_{1-x}VO₄ [8] exhibit extremely high single-pass gains (>1,000). They are useful for generating high-average-power outputs with high efficiencies in the picosecond regime without using a regenerative amplifier geometry. They are also capable of producing high-repetition rate (megahertz) pulses at a high cost efficiency.

A phase-conjugate master-oscillator power amplifier (PC-MOPA) system formed by bounce amplifiers and a phase-conjugate mirror can produce high output powers from such systems without degrading the beam quality by utilizing a self-aligned multipass geometry [9]. In recent years, we have demonstrated a high average output power (~26 W) with high beam quality ($M^2 < 1.5$) and an extraction efficiency of 35% from a PC-MOPA system based on a side-pumped Nd:YVO₄ bounce amplifier and a photorefractive phase-conjugate mirror formed from rhodium-doped barium titanate (Rh:BaTiO₃) [10,11]. Our system has the potential to be utilized in the above-mentioned applications.

In this present paper, we describe power scaling of a picosecond PC-MOPA system by cascading the phase-conjugate output to a second Nd:YVO₄ power amplifier. We also investigate the thermal effects in the second amplifier at various external incident angles with a view to minimizing degradation of the beam quality of the output from the second power amplifier. Using this system, 80.5 W picosecond output with a beam propagation factor of $M^2 < 1.8$ was demonstrated at a pulse repetition frequency (PRF) of 100 MHz. Generation of high-intensity megahertz pulses with peak powers of 7.4 MW and an average power of 78.5 W was also demonstrated by using a pulse picker formed from a rubidium titanyl phosphate (RTP) Pockels cell.

2. Experiments

2.1 PC-MOPA system

Figure 1 shows the experimental setup for the PC-MOPA system. The system is almost identical with those used in previous studies by us [11]. The master laser used for the system was a 200 mW continuous-wave (CW) mode-locked Nd:YVO₄ laser with a pulse duration of 6.3 ps and a PRF of 100 MHz. A 1 at.% Nd:YVO₄ slab (dimensions: 20 mm × 5 mm × 2 mm) was used for the amplifier and it was transversely pumped by a CW 808-nm diode array stack. The pump diode output was line-focused by a cylindrical lens (CLD) ($f = 25$ mm) on the pump face of the amplifiers.

The output pulses from the master laser were selected to have a PRF of 1.0 MHz by an external electro-optical modulator (EOM) synchronized with the pulses from the master laser. The master laser beam was focused to an elliptical spot by two cylindrical lenses, HCL₁ ($f = 500$ mm) and VCL ($f = 100$ mm), and it was then injected into the amplifier. This arrangement assured good spatial overlap between the master laser beam and the ellipsoidal gain volume in the amplifier. The powers of the master laser beam injected into the amplifier were respectively fixed to 12 and 2 mW at PRFs of 100 and 1.0 MHz to ensure that no depoling of the Rh:BaTiO₃ crystal occurred [12].

The amplified master laser beam was retroreflected by 4f imaging optics formed by two mirrors and a spherical lens L ($f = 100$ mm) causing it to re-enter the amplifier. The external

incident angles of the master laser beam and the amplified beam relative to the pump surface were 16° and 19° , respectively.

The amplified beam emerging from the amplifier was collimated by the two cylindrical lenses, VCL_1 ($f = 100$ mm) and HCL_2 ($f = 200$ mm), and it was then directed toward a Rh:BaTiO₃ crystal [13,14] by relay optics formed by two cylindrical lenses, HCL_3 ($f = 200$ mm) and HCL_4 ($f = 75$ mm). The polarization of the amplified beam was rotated using a half-wave plate HWP_2 so that it lay in the extraordinary plane of the Rh:BaTiO₃ crystal in order to achieve effective phase conjugation. The phase conjugate of the amplified beam was automatically fed-back to the amplifier. To prevent feedback to the master laser, an optical isolator was formed by a polarizing beam splitter (PBS), a Faraday rotator (FR), and a half-wave plate (HWP). In this manner, the phase conjugate beam, after passing twice through the amplifier, was ejected as output by the PBS.

The photorefractive crystal used was a 1000-ppm Rh-ion-doped BaTiO₃ crystal with dimensions of $8\text{ mm} \times 7\text{ mm} \times 8\text{ mm}$; it was 0° -cut to the normal to the c -axis. The crystal surfaces were AR-coated for $1\ \mu\text{m}$ to reduce surface reflection loss. The temperature of the crystal mount was maintained at $\sim 20^\circ\text{C}$. A ring phase-conjugate mirror was formed by the BaTiO₃ crystal and an external loop that contained a $4f$ imaging lens ($f = 150$ mm). The external loop angle was 15° and the loop was 600 mm long. Using this system, phase conjugation built up within a couple of minutes and it had a typical reflectivity of $\sim 50\%$.

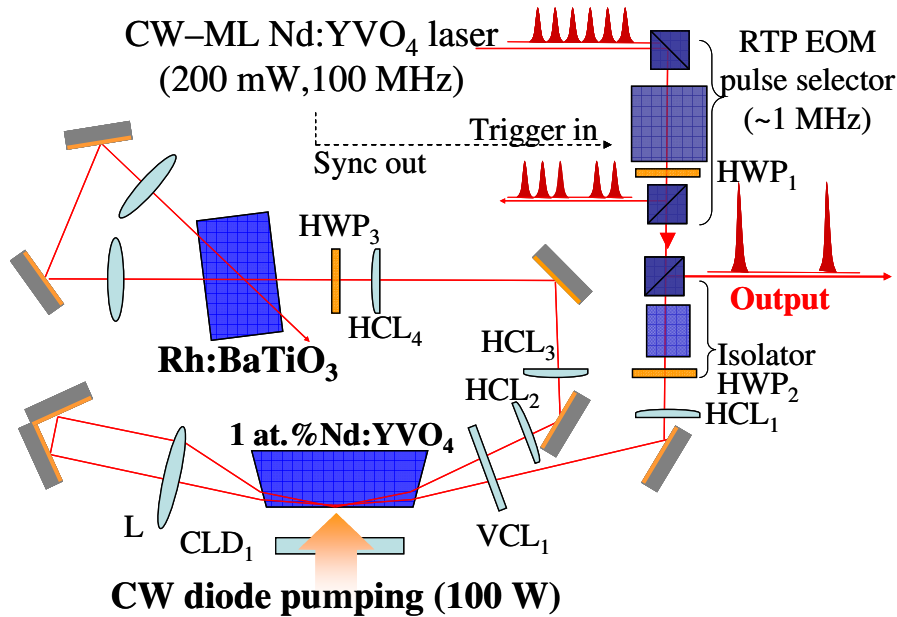


Fig. 1. Schematic diagram of the experimental setup of the PC-MOPA system.

Figure 2 shows the average output power in the PC-MOPA system as a function of the pump power. When the PRF was fixed to 100 MHz and the EOM was switched off, a maximum output power of 27.9 W was achieved at a pump power of 95 W. When the EOM was turned on, the laser started to operate at a PRF of 1 MHz. The actual input power to the amplifier was only ~ 2 mW. The amplifier in the PC-MOPA system was saturated even with such a weak input, and the output power reached 25.6 W at the maximum pump power.

The output from the system exhibited a near Gaussian spatial profile, and its corresponding beam-propagation factor, M^2 , was < 1.5 , while the M^2 of the incident amplified beam on the phase-conjugate mirror was ~ 3.1 . These results indicate that the system compensates for thermal distortions inside the amplifier.

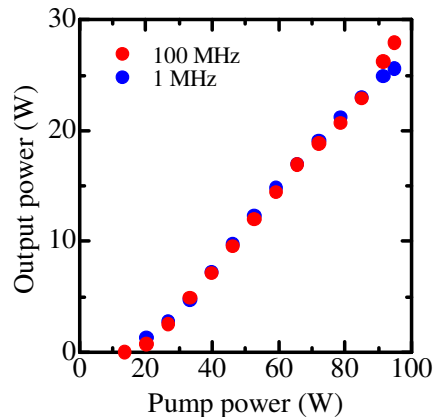


Fig. 2. Red circles are experimental output powers as a function of the pump power at PRF of 100 MHz. Blue circles are output powers at PRF of 1 MHz.

2.2 Cascading PC-MOPA output to second power amplifier

We combined a second power amplifier based on a side-diode-pumped 1 at.% Nd:YVO₄ slab with the PC-MOPA system [15]. Figure 3 shows a schematic diagram of this system. The pump power in the PC-MOPA system was fixed at 95 W. The slab used for the second amplifier was identical to that used for the PC-MOPA system. The second amplifier was also pumped by a fast-axis collimated CW diode array stack. To reduce the thermal lens in the second amplifier, the pump diode output was loosely focused by a cylindrical lens with a long focal length (CLD₂, $f = 50$ mm) onto the pump face.

The output from the PC-MOPA was focused by a cylindrical lens, VCL₂ ($f = 200$ mm), to be an elliptical spot with dimensions of 0.5 mm \times 1.5 mm, and it was cascaded to the second amplifier. The power injected into the second amplifier was sufficiently high (~ 21 W) to saturate it, resulting in highly efficient power extraction from the second amplifier. To prevent severe distortion of the amplified wavefront [12], we made the incident angle of the output from the PC-MOPA relatively large relative to the pump surface of the second amplifier ($\sim 23^\circ$).

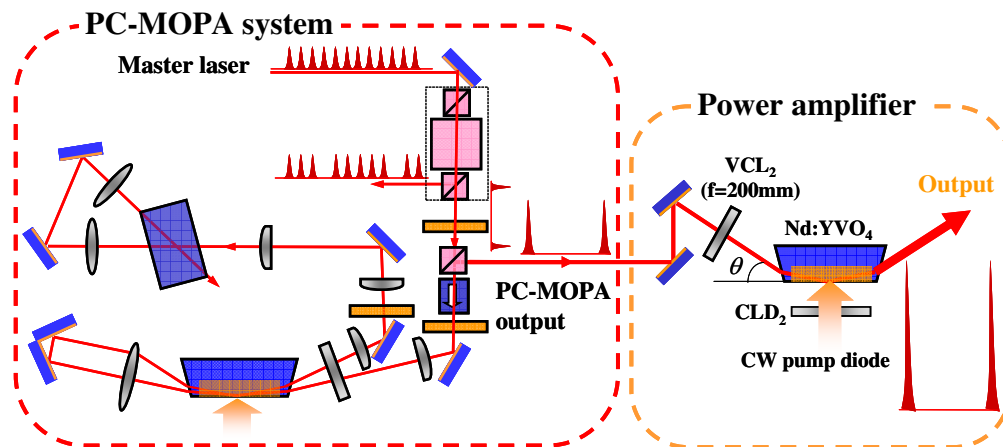


Fig. 3. Schematic diagram of the experimental setup of the second power amplifier.

Figure 4 shows the measured output power from the second amplifier as a function of pump power. The PRF, first, was fixed to be 100 MHz. A maximum output power of 80.5 W was obtained at a pump power of ~ 135 W, and the corresponding gain of the second amplifier

was estimated to be ~ 2.9 . An extraction efficiency of $>40\%$ was measured in the second amplifier. Figure 5(a) shows an intensity autocorrelation trace of the output. The output from the second amplifier had a pulse width of 9.2 ps for a Gaussian-shaped pulse, while the output from the PC-MOPA exhibited a pulse duration (FWHM) of 7.6 ps. This slight pulse broadening is induced by saturation effects due to the finite gain band (~ 1 nm) of the amplifier. The temporal evolution of the output is shown in Fig. 5(b). The standard deviation of the peak power fluctuations in the output was estimated to be $\sim 1\%$.

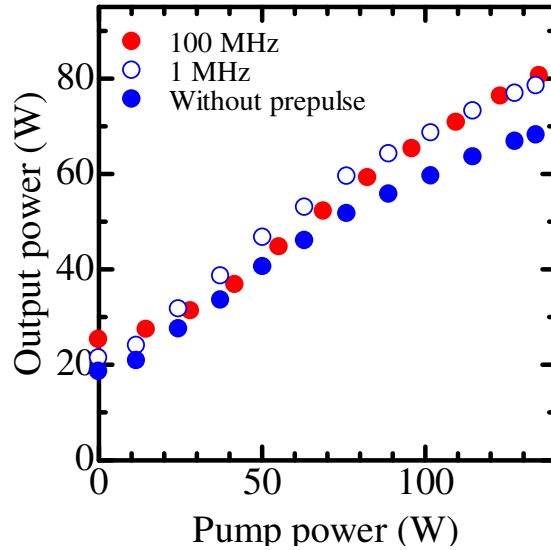


Fig. 4. Red circles indicate the experimentally measured average output power as a function of the pump power at a PRF of 100 MHz. Blue open and filled circles also show the average powers with and without prepulses at a PRF of 1 MHz.

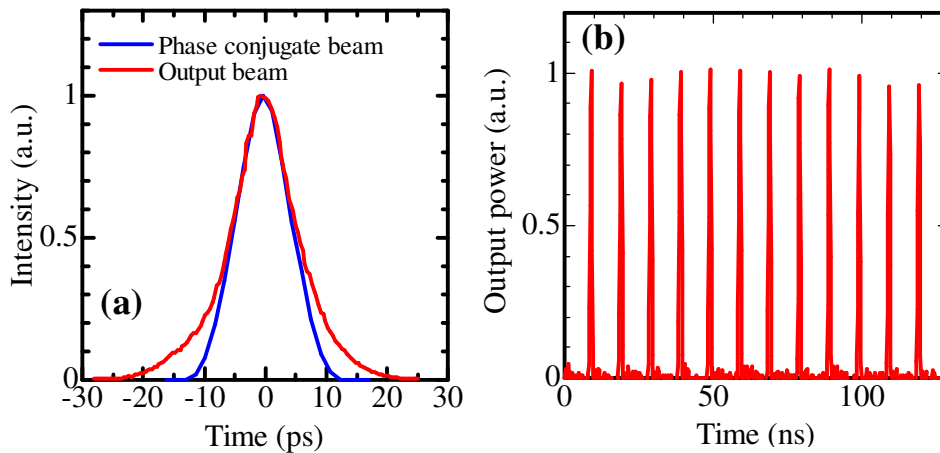


Fig. 5. (a) Blue and red curves are the intensity autocorrelation traces of the PC-MOPA output and amplified output from the second amplifier, respectively. (b) The temporal evolution of the output at the PRF of 100 MHz.

We also measured the temporal behaviors of average power of the output from the system during a long observation time. The pump power was fixed to 135 W. As shown in Fig. 6, the system exhibited excellent temporal stability, and the standard deviations of the fluctuations in average power of the output over 35 minutes was estimated to be $< 1\%$. The output from the

second amplifier had a near Gaussian spatial profile in the far-field (Fig. 7), and its horizontal beam-propagation factor, M^2 , was <1.8 .

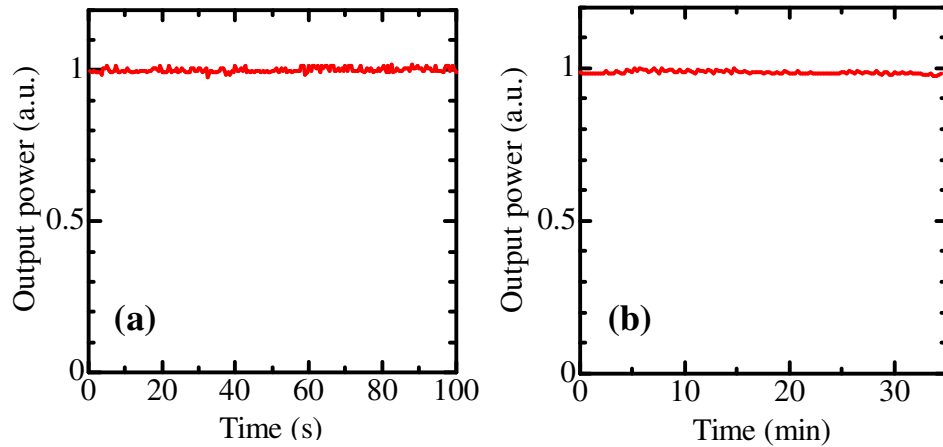


Fig. 6. Temporal evolution of average power of the output from the second amplifier at the maximum pump power. (a) Experimental average power measured at intervals of 0.5 second.. (b) Measured average power over 35 minutes at 15 second intervals.

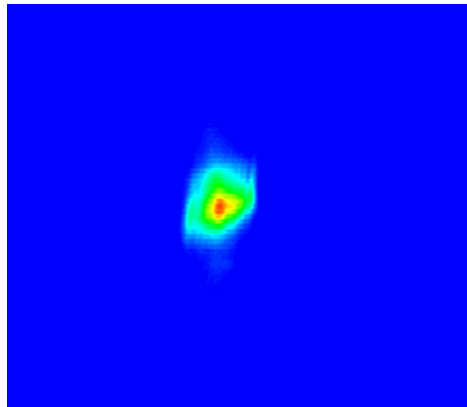


Fig. 7. The spatial profile of the output beam from the second amplifier.

When the EOM was turned on to give a PRF of 1 MHz, the output power was measured to be 78.5 W. The temporal evolution of the amplified pulses at a PRF of 1 MHz is shown in Fig. 8(a). The standard deviation of the peak power fluctuations in the output was estimated to be $<2\%$. As previously related [11], the output from the system contained undesirable amplified prepulses along with the main output pulses. Figure 8(b) also shows that the ratio of the peak powers of the undesired prepulse to the main pulse was measured to be ~ 0.0015 ($\sim 1:660$). Accordingly, the output power without the prepulses was estimated to be 68.2 W. The corresponding peak power of the main pulses was estimated to be 7.4 MW by using the average power, the pulse width, and the pulse contrast ratio (Fig. 4). This value is ~ 83 times higher than that at a PRF of 100 MHz. The beam quality of the output was almost same as that at a PRF of 100 MHz.

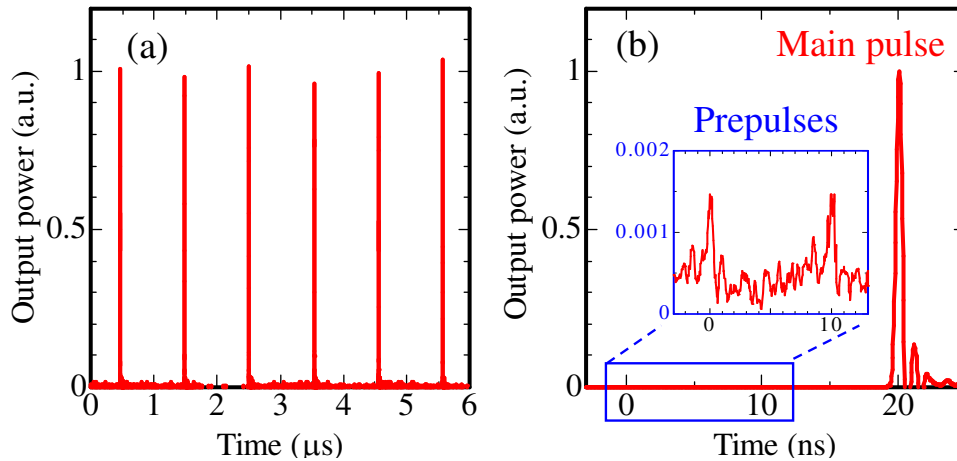


Fig. 8. (a) Temporal profile of the amplified pulses at a PRF of 1 MHz. (b) An enlargement of the temporal evolution of the main and undesired pulses. The contrast ratio of the undesired prepulse to the main pulse was estimated to be $\sim 1:660$.

3. Discussion

Line focus pumping in a side-pumped bounce amplifier produces an astigmatic thermal lens in the slab. In particular, the phase distribution in the horizontal direction in the amplifier is an exponential curve that includes higher-order terms related to effective aberrations, while the phase distribution in the vertical direction is a parabolic curve involving a lens effect that can be easily compensated for using a cylindrical lens. Thus, the amplified output is frequently distorted in the horizontal direction through the amplifier.

To estimate the phase aberration in the horizontal direction in the second amplifier, we numerically simulated the phase distribution in the second amplifier by using a conventional heat diffusion equation [16,17]. We assumed that the thermal load in the amplifier was mainly induced by the energy quantum defect between the pump and laser photons, and the heat in the pump region ($18 \times 0.3 \text{ mm}^2$) on the slab was removed by conduction cooling on the top and bottom faces ($20 \times 5 \text{ mm}^2$) of the slab. Figure 9 shows the numerically simulated model.

The spatial distribution of the phase shift that the injected beam with a beam size of $\sim 1.5 \text{ mm}$ experienced in the second amplifier at various external incident angles θ is also shown in Fig. 9. It was found by integrating the phase shift, defined as the product of the temperature rise and the thermo-optic coefficient dn/dT ($3.0 \times 10^{-6}/\text{K}$) [18], along the optical axis x' .

Figure 10(a) shows the simulated phase distribution $\phi(y)$ at an external incident angle of 23° . The red curve in Fig. 10(a), found by fitting the spatial distribution $\phi(y)$ with a parabolic function, represents the thermal lens term. We estimated the higher-order terms related to effective aberrations by subtracting the thermal lens term from the simulated phase distribution $\phi(y)$ (Fig. 10(b)).

As the external incident angle to the second amplifier increases, the effective aberrations decrease significantly. Above an external angle of 23° , the phase difference between the maxima and minima values is less than 0.3 rad ($\lambda/10$), so that the amplified output does not affect phase aberration. There is a good consistency between the simulations and experiments.

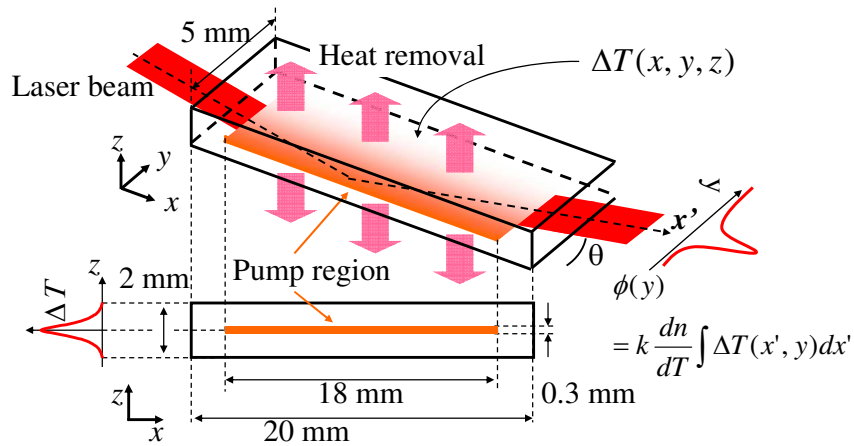


Fig. 9. Numerically simulated model of the phase shift of the bounce amplifier. ΔT is the temperature distribution.

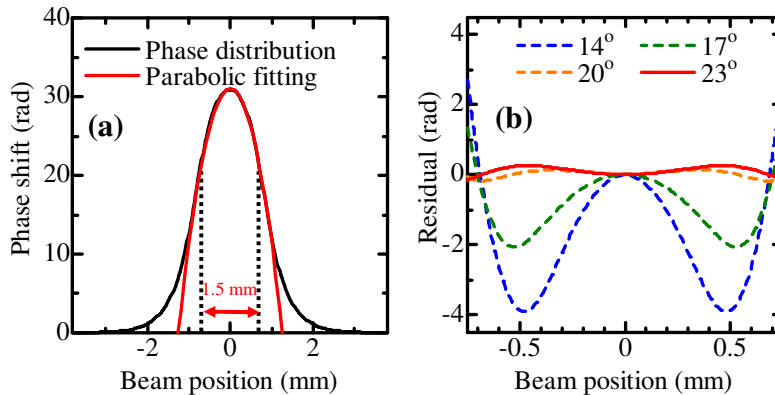


Fig. 10. (a) The black curve indicating the phase distribution passing through the amplifier and the red curve is the parabolic fit for a beam size of 1.5 mm. (b) Numerically calculated phase aberrations for four different external angles.

4 Conclusions

We investigated power scaling in a phase-conjugate Nd:YVO₄ bounce amplifier by using a cascaded diode-side-pumped Nd:YVO₄ bounce amplifier geometry. Average output powers of 80.5 and 78.5 W were achieved at PRFs of 100 and 1 MHz, respectively. The corresponding peak power at a PRF of 1 MHz was 7.4 MW. The overall power extraction efficiency of the whole system was >35%. The standard deviation of the peak power fluctuations in the output was measured to be <2%. And the temporal stability of the output during a long observation time of 35 minutes also had the fluctuations of 0.5%. To the best of our knowledge, these values are the highest obtained using a bounce amplifier in combination with a phase-conjugate mirror in the picosecond regime. The output exhibited a pulse duration (FWHM) of 9.2 ps and a M^2 of <1.8. Further power scaling up to >100 W should be possible by optimizing the pump diodes (for example, by using 880-nm pump diodes to reducing the heat loading in the amplifier).

Acknowledgement

The authors acknowledge support from a Scientific Research Grant-in-Aid (19018007, 18360031) from the Ministry of Education, Science and Culture of Japan and the Japan Society for the Promotion of Science.